THE JOURNAL OF PHYSICAL CHEMISTRY C

Article

Cite This: J. Phys. Chem. C 2018, 122, 24467−24474

pubs.acs.org/JPCC

Can Raman Shift Be Used To Characterize the Mechanical Property of Graphene?

Kathleen L. Yang,[†] Jeong Oen Lee,[†] Hyuck Choo,*[,†,‡] and Fuqian Yang*[,§]

[†]Department of Electrical Engineering and [‡]Cherng Department of Medical Engineering, California Institute of Technology, Pasadena, California 91125, United States

[§]Materials Program, Department of Chemical and Materials Engineering, University of Kentucky, Lexington, Kentucky 40506, United States

ABSTRACT: Graphene has potential in a variety of applications, including strain-engineering electronics and sensors. In the heart of these applications is the strain dependence of electronic properties associated to the strain-induced Raman shift of graphene. In this work, we extend the relationship between the Raman shift of strained graphene and the mechanical strains for uniaxial tension to three-dimensional strain state and analyze the bending-induced Raman shift of orthotropic, monolayer graphene of rectangular and elliptic shapes, respectively, under the action of uniform pressure. The results show that the largest Raman redshift is present at the center of the graphene for both geometric configurations, and there exists Raman blueshift near the edges of the graphene. For both geometrical configurations, the contours of the Raman shift around the center are present in the shape of ellipse, which is dependent on the boundary conditions and geometrical configurations of the graphene. The geometric shape of the contours of the Raman shift likely cannot represent the anisotropic behavior in the mechanical deformation of graphene, and the initial state and constitutive relationship of graphene are needed to characterize the mechanical property of graphene via the strain-induced Raman shift.

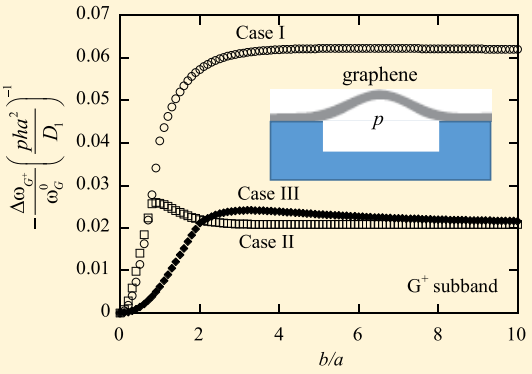

INTRODUCTION

Graphene is a two-dimensional (2D) material with potential applications in electronics, photonics, energy storage, etc. Graphene exhibits the strain dependence of electronic properties,[1,2] which makes it possible to build electronic circuits from graphene only with different electronic components (graphene) being at different states of strains[1,3] and graphene-based sensors.[4] To utilize the coupling between straining and electronic properties of graphene for the applications in electronics and sensors, it is of practical importance to characterize the strain state of graphene and understand the dependence of electronic and optical properties of graphene on the strain state.

It is known that straining a crystal can cause the wavenumber change of crystal phonon and the change of the energy spectrum of nanostructures[5] due to the strain dependence of the anharmonicity of the interatomic potentials of atoms.[6] Raman spectrum has been well established to quantitatively measure strain/stress in crystalline semiconductors because of the strain dependence of the wavenumber change of crystal phonon. There are reports on the experimental study of the correlation between the Raman shift and the strain in graphene. In general, the methods used to deform the graphene can fall into two categories: one is the tension test and the other is the bending test. Raman spectroscopy is then used to study the variation of the Raman shift with the strain in graphene. Huang et al.[7] studied the Raman spectra of optical phonons in graphene monolayers under uniaxial tensile stress and observed red shifts of both the G and 2D bands. del Corro et al.[8] used the Raman 2D′ mode to measure the strain in graphene, which was placed on poly(methyl methacrylate) (PMMA) substrate and experienced "tensile" strain due to the bending of the PMMA substrate. Placing a monolayer graphene on polyethylene terephthalate, Jiang et al.[9] observed tension-induced blueshift of the Raman peaks of the graphene. Mohiuddin et al.[10] used the bending method to deform graphene for analyzing strain-induced splitting of G peak and the Grüneisen parameters of graphene. Using the shifts of the Raman peaks, Lee et al.[11] calculated Young's modulus of graphene via pressure-induced inflation of a graphene membrane. Zable et al.[3] pointed out that there exists interaction between substrate and graphene, which can introduce mechanical strain in graphene and lead to a discrepancy in the Raman shift. They used graphene bubbles and balloons in the analysis of Raman spectroscopy. Using three-point bending to introduce biaxial strain to graphene flakes, Androulidakis et al.[12] calculated the Grüneisen parameters for the G and 2D peaks from the Raman shifts.

Received: August 16, 2018
Revised: October 1, 2018
Published: October 2, 2018

DOI: 10.1021/acs.jpcc.8b07996
J. Phys. Chem. C 2018, 122, 24467−24474

All these analyses have been based on graphene being isotropic. It needs to be pointed out that the Grüneisen parameters for the G and 2D bands of graphene have been reported to be in a range of 1.8−2.4 and 2.4−3.8, respectively, which may be dependent on the stress state of the graphene.

Using molecular dynamics, Ni et al.[13] revealed anisotropic−mechanical properties of a sheet of graphene, which can be attributed to the hexagonal structure of graphene. Settembrini et al.[14] suggested that graphene behaves anisotropically from two-dimensional analysis of Raman shifts via the deflection of a graphene monolayer anchored to SiN holes of noncircular geometry. Their results raise the issue: whether the Raman shift can reveal the anisotropic behavior of the mechanical deformation of graphene. Also, both results point to the anisotropic characteristics of graphene, which need to be incorporated in the analysis of the strain dependence of the Raman shift of graphene. There are analyses on the deformation of graphene, in which the graphene was modeled as orthotropic.[15,16] Considering the potential applications of graphene, we assume graphene as orthotropic and analyze the effect of bending deformation on the Raman shift of graphene in this work. The strain-induced Raman shift of graphene under uniaxial loading is first extended to three-dimensional loading. Two geometric configurations are then considered for the bending-induced Raman shift of orthotropic, monolayer graphene.

STRAIN-INDUCED RAMAN SHIFT OF GRAPHENE

It is known that deformation can cause the G band to split into the G^- and G^+ bands and the 2D band to shift in the same direction as the G band.[8,17,18] The 2D band exhibits different broadening and splitting under uniaxial strain from the G band.[8,19] The deformation-induced shift of the G sub-bands of graphene can be expressed as[10]

$$\Delta\omega_{G^\pm} = \Delta\omega_G^h \pm \frac{1}{2}\Delta\omega_G^s \tag{1}$$

in which the first term represents the shift due to volumetric strain and the second term represents the mode splitting due to the effective shear strain. Here, $\Delta\omega_{G^\pm} = \omega_{G^\pm} - \omega_G^0$ with $\omega_{G^\pm}$ being the wavenumbers of the Raman peaks of the $G^\pm$ sub-bands and ω_G^0 being the wavenumber of the Raman peak of the G band at stress-free state.

For a three-dimensional strain state, the volumetric strain, ε_V, is calculated as

$$\varepsilon_V = \varepsilon_{xx} + \varepsilon_{yy} + \varepsilon_{zz} \tag{2}$$

and the maximum shear strain, ε_{max}, can be calculated as

$$\varepsilon_{max} = \frac{1}{2}\max[|\varepsilon_1 - \varepsilon_2|, |\varepsilon_2 - \varepsilon_3|, |\varepsilon_1 - \varepsilon_3|] \tag{3}$$

where ε_1, ε_2, and ε_3 are the principal strains. The volumetric strain represents the volumetric change created by hydrostatic stress, and the maximum shear strain is associated to shape distortion. For the uniaxial tension of isotropic material, eq 3 gives

$$\varepsilon_{max} = \frac{1}{2}|\varepsilon_{||} - \varepsilon_{tt}| \tag{4}$$

which is similar to the result used by del Corro et al.[8] with a coefficient of 1/2. For biaxial deformation of monolayer graphene, assume that the transverse strain is negligible and $\varepsilon_{zz} \approx 0$. Equations 2 and 3 become

$$\varepsilon_V = \varepsilon_{xx} + \varepsilon_{yy}, \text{ and } \varepsilon_{max} = \frac{1}{2}\max[|\varepsilon_{xx} + \varepsilon_{yy} \pm \sqrt{(\varepsilon_{xx} - \varepsilon_{yy})^2 + \gamma_{xy}^2}|, \sqrt{(\varepsilon_{xx} - \varepsilon_{yy})^2 + \gamma_{xy}^2}] \tag{5}$$

with γ_{xy} $(=2\varepsilon_{xy})$ being the shear strain. According to the relationship given by Mohiuddin et al.[10] and del Corro et al.,[8] the shifts of the G sub-bands can be expressed as

$$\Delta\omega_{G^\pm} = -\gamma_G\omega_G^0(\varepsilon_{xx} + \varepsilon_{yy}) \pm \beta_G\omega_G^0\varepsilon_{max} \tag{6}$$

with ω_G^0 being the wavenumber of the G band at stress-free state. The parameters of γ_G and β_G are the G mode's Grüneisen parameter and shear deformation potential, respectively, which can be calculated from the in-plane Raman-active E_{2g} phonon as[10,11]

$$\gamma_G = -\frac{1}{\omega_G^0}\frac{\partial\omega_G}{\partial\varepsilon_v} \text{ and } \beta_G = \frac{1}{\omega_G^0}\frac{\partial\omega_G}{\partial\varepsilon_{max}} \tag{7}$$

where ω_G is the wavenumber of the Raman peak of the G band of strained graphene depending on the volumetric strain and shear strain.

For the 2D′ mode of graphene, which is associated with two LO-derived phonons from the vicinity of the Γ point, eq 1 can be used to describe the relationship between the strain-induced shift of the wavenumber of the sub-bands under the action of uniaxial tension with the ω_G^0 being replaced by $\omega_{2D'}^0$ and the corresponding terms of γ_G and β_G being replaced by γ_{2D} and β_{2D}, respectively. Assuming that this relationship can be used in graphene experiencing in-plane deformation, we have

$$\Delta\omega_{2D'} = -\gamma_{2D}\omega_{2D'}^0(\varepsilon_{xx} + \varepsilon_{yy}) \pm \beta_{2D}\omega_{2D'}^0\varepsilon_{max} \tag{8}$$

which reduces to the result given by Narula et al.[20] Here, the parameters of γ_{2D} and β_{2D} are calculated as

$$\gamma_{2D} = -\frac{1}{\omega_{2D'}^0}\frac{\partial\omega_{2D'}}{\partial\varepsilon_v} \text{ and } \beta_{2D} = \frac{1}{\omega_{2D'}^0}\frac{\partial\omega_{2D'}}{\partial\varepsilon_{max}} \tag{9}$$

where $\omega_{2D'}$ is the 2D′ mode wavenumber of strained graphene depending on the volumetric strain and shear strain.

It is worth pointing out that eqs 6 and 8 are based on the assumption that the initial state of the graphene is stress free. For a prestretched (predeformed) graphene, assume that the superposition principle can be used to calculate the final deformation state of the graphene. Both eqs 6 and 8 can be extended to the prestretched (predeformed) graphene as

$$\Delta\omega_{G^\pm} = \omega_{G^\pm} - \omega_G^p = -\gamma_G^p\omega_G^p\Delta(\varepsilon_{xx} + \varepsilon_{yy}) \pm \beta_G^p\omega_G^p\Delta\varepsilon_{max} \tag{10}$$

$$\Delta\omega_{2D'} = \omega_{2D'} - \omega_{2D'}^p = -\gamma_{2D}^p\omega_{2D'}^p\Delta(\varepsilon_{xx} + \varepsilon_{yy}) \pm \beta_{2D}^p\omega_{2D'}^p\Delta\varepsilon_{max} \tag{11}$$

in which the wavenumbers with the superscript of p represent those at the prestretched (predeformed) state and $\Delta(\varepsilon_{xx} + \varepsilon_{yy})$ and $\Delta\varepsilon_{max}$ are the changes of the volumetric strain and maximum shear strain, respectively. According to eqs 10 and 11, we note that the Raman shift is dependent on the initial stress state of graphene and both the Grüneisen parameter and shear deformation potential are likely dependent on the prestretched (predeformed) state. Extending eqs 7 and 9 to prestrained graphene, we have

DOI: 10.1021/acs.jpcc.8b07996
J. Phys. Chem. C 2018, 122, 24467−24474

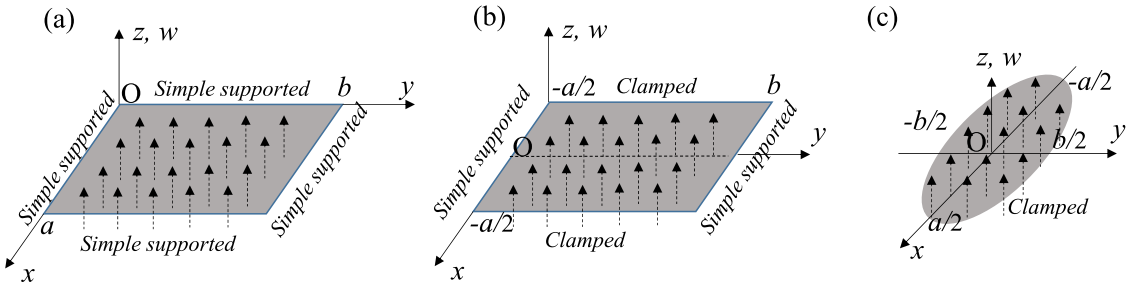

Figure 1. Geometric configurations of the bending of graphene; (a) rectangular graphene with simply supported edges, (b) rectangular graphene with two simply supported and two clamped edges, and (c) elliptic graphene clamped along the edge.

$$(\gamma_G^P, \gamma_{2D}^P) = -\left(\frac{1}{\omega_G^P}\frac{\partial\omega_G}{\partial\varepsilon_v}\bigg|_{\omega_G=\omega_G^P}, \frac{1}{\omega_{2D'}^P}\frac{\partial\omega_{2D'}}{\partial\varepsilon_v}\bigg|_{\omega_{2D'}=\omega_{2D'}^P}\right) \tag{12}$$

$$(\beta_G^P, \beta_{2D}^P) = \left(\frac{1}{\omega_G^P}\frac{\partial\omega_G}{\partial\varepsilon_{max}}\bigg|_{\omega_G=\omega_G^P}, \frac{1}{\omega_{2D'}^P}\frac{\partial\omega_{2D'}}{\partial\varepsilon_{max}}\bigg|_{\omega_{2D'}=\omega_{2D'}^P}\right) \tag{13}$$

For ω_G and $\omega_{2D'}$ being linear functions of volumetric strain and maximum shear strain, eqs 10 and 11 are similar to eqs 6 and 8. The co-efficients for the Raman shifts are independent of the prestretched (predeformed) state.

Substituting eqs 12 and 13 into eqs 10 and 11 yields

$$\begin{pmatrix}\Delta\omega_{G^\pm}\\ \Delta\omega_{2D'}\end{pmatrix} = \Delta(\varepsilon_{xx}+\varepsilon_{yy})\begin{pmatrix}\frac{\partial\omega_G}{\partial\varepsilon_v}\big|_{\omega_G=\omega_G^P}\\ \frac{\partial\omega_{2D'}}{\partial\varepsilon_v}\big|_{\omega_{2D'}=\omega_{2D'}^P}\end{pmatrix} \pm \Delta\varepsilon_{max}\frac{\partial}{\partial\varepsilon_{max}}\begin{pmatrix}\frac{\partial\omega_G}{\partial\varepsilon_{max}}\big|_{\omega_G=\omega_G^P}\\ \frac{\partial\omega_{2D'}}{\partial\varepsilon_{max}}\big|_{\omega_{2D'}=\omega_{2D'}^P}\end{pmatrix} \tag{14}$$

One can note that the Raman shifts in eq 14 with the summation sign ("+") are the first-order Taylor expansions of ω_G and $\omega_{2D'}$, which is applicable to small changes in the strains. For large strains, higher-order terms with the derivative of the Grüneisen parameter and shear deformation potential likely need to be included in the calculation.

BENDING DEFORMATION OF ORTHOTROPIC GRAPHENE

For orthotropic graphene with the direction of x- and y-axes coinciding with the principal directions of elasticity, the relationship between stress and strain can be expressed as

$$\varepsilon_{xx} = \frac{1}{E_1}(\sigma_x - \nu_1\sigma_y),\ \varepsilon_{yy} = \frac{1}{E_2}(\sigma_y - \nu_2\sigma_x),\ \text{and}\ \gamma_{xy} = \frac{1}{G}\sigma_{xy} \tag{15}$$

Here, (ε_{xx}, ε_{yy}, γ_{xy}) are the components of strain tensor, (σ_x, σ_y, σ_{xy}) are the components of stress tensor, and (E_1, E_2, ν_1, ν_2, G) are the Young's moduli, Poisson's ratios and shear modulus for the principal directions. Note, $E_1\nu_2 = E_2\nu_1$.

For small deformation, the linear plate theory is used. The equation for the deflection, w, of the orthotropic graphene of h in thickness under the action of pressure of p with the direction of x- and y-axes coinciding with the principal directions is

$$D_1\frac{\partial^4 w}{\partial x^4} + 2D_3\frac{\partial^4 w}{\partial x^2\partial y^2} + D_2\frac{\partial^4 w}{\partial y^4} = p \tag{16}$$

where

$$D_1 = \frac{E_1h^3}{12(1-\nu_1\nu_2)},\ D_2 = \frac{E_2h^3}{12(1-\nu_1\nu_2)},\ \text{and}\ D_3 = \frac{\nu_2E_1h^3}{12(1-\nu_1\nu_2)} + \frac{Gh^3}{6} \tag{17}$$

The strain components in the graphene can be calculated from the deflection of the graphene as

$$\varepsilon_{xx} = -\frac{h}{2}\frac{\partial^2 w}{\partial x^2},\ \varepsilon_{yy} = -\frac{h}{2}\frac{\partial^2 w}{\partial y^2},\ \text{and}\ \gamma_{xy} = -h\frac{\partial^2 w}{\partial x\partial y} \tag{18}$$

In the following analysis, we only consider the cases with closed-form solutions. For detailed derivation, see the work by Panc.[21]

Case I: Bending of a Rectangular Orthotropic Graphene with Simply Supported Edges. Figure 1a shows a rectangular orthotropic graphene with the principal directions parallel to corresponding sides and all edges being hinged under the action of a uniform pressure of p. The deflection of the graphene is

$$w = \frac{16pb^4}{\pi^6}\sum_{m=1}^{\infty}\sum_{n=1}^{\infty}a_{mn}\sin[(2m-1)\pi x/a]\sin[(2n-1)\pi y/b] \tag{19}$$

with

$$\alpha_{mn} = \frac{(2n-1)^{-1}(2m-1)^{-1}}{D_1[(2m-1)b/a]^4 + 2D_3(2n-1)^2[(2m-1)b/a]^2 + D_2(2n-1)^4} \tag{20}$$

for $0 \le x \le a$ and $0 \le y \le b$. From eq 19, the normal components of the strain tensor on the top surface of the graphene are

$$\varepsilon_{xx} = \frac{8hpb^4}{\pi^4}\sum_{m=1}^{\infty}\sum_{n=1}^{\infty}\frac{(2m-1)^2\alpha_{mn}}{a^2}\sin[(2m-1)\pi x/a]\sin[(2n-1)\pi y/b] \tag{21}$$

DOI: 10.1021/acs.jpcc.8b07996
J. Phys. Chem. C 2018, 122, 24467−24474

Table 1. Material Properties of Orthotropic, Monolayer Graphene

E_1 (GPa)	ν_1	E_2 (GPa)	ν_2	G (GPa)	h (nm)	ω_G^0 (cm^{-1})	γ_G	β_G
1060[15]	0.3[15]	1030[15]	0.31	280[22]	0.34	1580[3]	1.99[8]	0.99[8]

$$\varepsilon_{yy} = \frac{8hpb^2}{\pi^4}\sum_{m=1}^{\infty}\sum_{n=1}^{\infty}(2n-1)^2\alpha_{mn}\sin[(2m-1)\pi x/a]\sin[(2n-1)\pi y/b] \quad (22)$$

Case II: Bending of a Rectangular Orthotropic Graphene with Two Simply Supported Edges and Two Clamped Edges. Figure 1b shows a rectangular orthotropic graphene with the principal directions parallel to corresponding sides under the action of a uniform pressure of p. One pair of opposite edges is hinged, and the other pair is clamped. The deflection of the graphene is

$$w = \frac{p}{24D_2}(y^4 - 2by^3 + b^3y) + \frac{4pb^4}{D_2\pi^5}\sum_{n=1}^{\infty}\frac{1}{(2n-1)^5\beta_n}\sin\frac{(2n-1)\pi y}{b}\cdot\left(s_2\sinh\frac{(2n-1)\pi s_2 a}{2b}\cosh\frac{(2n-1)\pi s_1 x}{b} - s_1\sinh\frac{(2n-1)\pi s_1 a}{2b}\cosh\frac{(2n-1)\pi s_2 x}{b}\right) \quad (23)$$

with

$$\beta_n = \left(s_1\sinh\frac{(2n-1)\pi s_1 a}{2b}\cosh\frac{(2n-1)\pi s_2 a}{2b} - s_2\sinh\frac{(2n-1)\pi s_2 a}{2b}\cosh\frac{(2n-1)\pi s_1 a}{2b}\right) \quad (24)$$

for $-a/2 \le x \le a/2$ and $0 \le y \le b$. The parameters of s_1 and s_2 are the roots of the following equation

$$D_1 s^4 - 2D_3 s^2 + D_2 = 0 \quad (25)$$

From eq 23, the normal components of the strain tensor on the top surface of the graphene are

$$\varepsilon_{xx} = \frac{2hpb^2 s_2 s_1}{D_2\pi^3}\sum_{n=1}^{\infty}\frac{1}{(2n-1)^3\beta_n}\sin\frac{(2n-1)\pi y}{b}\cdot\left(s_1\sinh\frac{(2n-1)\pi s_2 a}{2b}\cosh\frac{(2n-1)\pi s_1 x}{b} - s_2\sinh\frac{(2n-1)\pi s_1 a}{2b}\cosh\frac{(2n-1)\pi s_2 x}{b}\right) \quad (26)$$

$$\varepsilon_{yy} = \frac{phy}{4D_2}(y-b) - \frac{2phb^2}{D_2\pi^3}\sum_{n=1}^{\infty}\frac{1}{(2n-1)^3\beta_n}\sin\frac{(2n-1)\pi y}{b}\cdot\left(s_2\sinh\frac{(2n-1)\pi s_2 a}{2b}\cosh\frac{(2n-1)\pi s_1 x}{b} - s_1\sinh\frac{(2n-1)\pi s_1 a}{2b}\cosh\frac{(2n-1)\pi s_2 x}{b}\right) \quad (27)$$

Case III: Bending of an Elliptic Orthotropic Graphene with Clamped Edge. Figure 1c shows an elliptic orthotropic graphene with clamped edge under the action of a uniform pressure of p. Let x and y be the elliptic axes parallel to the principal directions of elasticity and the semiaxes be $a/2$ and $b/2$. The deflection of the elliptic orthotropic graphene is

$$w = \frac{pa^4}{8(3D_1 + 2D_3a^2/b^2 + 3D_2a^4/b^4)}\left(\frac{1}{4} - \frac{x^2}{a^2} - \frac{y^2}{b^2}\right)^2 \quad (28)$$

for $-a/2 \le x \le a/2$ and $-b/2 \le y \le b/2$. From eq 25, the normal components of the strain tensor on the top surface of the graphene are

$$\varepsilon_{xx} = -\frac{pha^2}{4(3D_1 + 2D_3a^2/b^2 + 3D_2a^4/b^4)}\left(\frac{1}{4} - \frac{3x^2}{a^2} - \frac{y^2}{b^2}\right) \quad (29)$$

$$\varepsilon_{yy} = -\frac{pha^4}{4b^2(3D_1 + 2D_3a^2/b^2 + 3D_2a^4/b^4)}\left(\frac{1}{4} - \frac{x^2}{a^2} - \frac{3y^2}{b^2}\right) \quad (30)$$

From eqs 21, 22, 26, 27, 29, and 30, we can note that the strain components are proportional to the pressure difference across the graphene and inversely proportional to the Young's moduli.

BENDING-INDUCED RAMAN SHIFT OF ORTHOTROPIC GRAPHENE

According to eqs 6 and 8, we can analyze the deformation-induced Raman shift of graphene with the initial state being deformation free, if the deformation state of the graphene is known. As mentioned in the introduction, the methods used to deform graphene can fall into two categories: one is the tension test and the other is the bending test. Raman spectroscopy is then used to study the variation of the Raman shift with the strain in graphene. Here, we only consider the bending deformation of graphene under the action of constant pressure and assume both the Grüneisen parameter and shear deformation potential being independent of the deformation of graphene. This assumption is based on that there are no data available in the literature for the strain dependence of either the Grüneisen parameter or shear deformation potential as well as one assumes that both the Grüneisen parameter and shear deformation potential are constant for small strain.

For graphene covering and sealing a cavity in a "rigid" substrate, constant pressure difference across the graphene can cause the deflection of the graphene. Assuming that deflection of the graphene can be described by the linear bending theory, we can use the results in the above section to analyze the bending-induced Raman shift of orthotropic graphene.

Considering the similarity of the mathematical expressions of the Raman shift of graphene between the G sub-bands and the 2D′ band, we only analyze the bending-induced Raman shift of the G sub-bands of orthotropic graphene for the three configurations discussed in the above section. Table 1 lists the parameters used in the analysis, in which ν_2 is calculated from

DOI: 10.1021/acs.jpcc.8b07996
J. Phys. Chem. C 2018, 122, 24467−24474

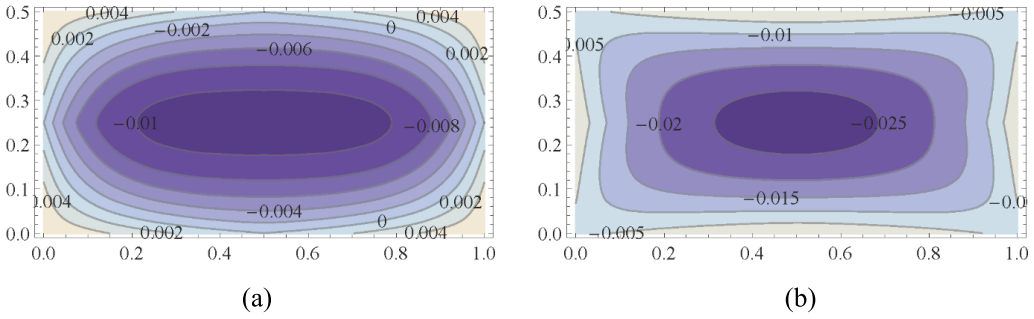

Figure 2. Contours of the bending-induced Raman shift ($\Delta\omega_{G^{\pm}} D_1/\omega_G^0 pha^2$) of an orthotropic−rectangular graphene with simply supported edges for $a/b = 2$; (a) G^+ sub-band, and (b) G^- sub-band.

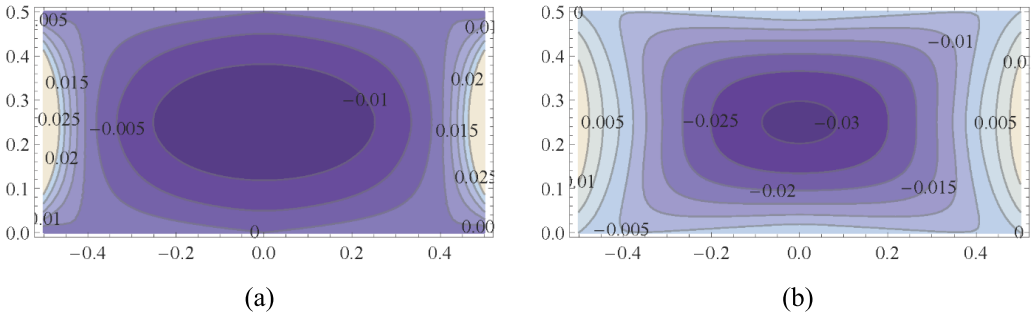

Figure 3. Contours of the bending-induced Raman shift ($\Delta\omega_{G^{\pm}} D_1/\omega_G^0 pha^2$) of an orthotropic−rectangular graphene with two simply supported and two clamped edges for $a/b = 2$; (a) G^+ sub-band and (b) G^- sub-band.

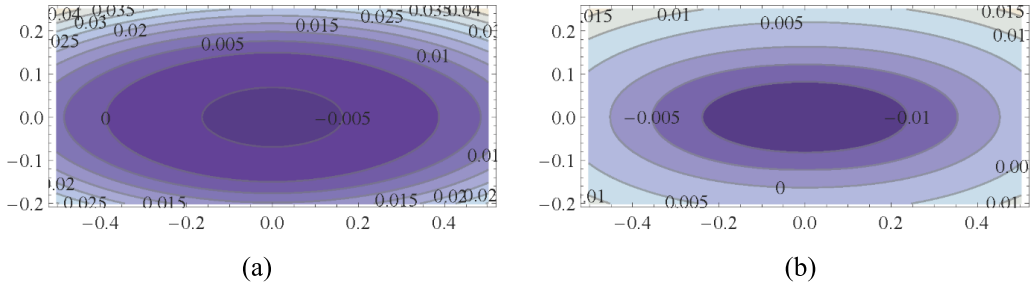

Figure 4. Contours of the bending-induced Raman shift ($\Delta\omega_{G^{\pm}} D_1/\omega_G^0 pha^2$) of an orthotropic−elliptic graphene clamped along the edge for $a/b = 2$; (a) G^+ sub-band and (b) G^- sub-band.

the relationship of $E_1\nu_2 = E_2\nu_1$. Note that there is no significant difference between E_1 and E_2, whereas the experimental value of G reported by Liu et al.[22] is significantly different from the value calculated from $E/2(1 + \nu)$. This trend likely suggests that either graphene is anisotropic or the properties of graphene are processing-dependent.

Figure 2 shows the contours of the bending-induced Raman shift of a rectangular orthotropic graphene with simply supported edges under the action of a uniform pressure for $a/b = 2$, in which normalized Raman shift of $\Delta\omega_{G^{\pm}} D_1/\omega_G^0 pha^2$ is used. The contours of the Raman shift near the center are present approximately in the shape of ellipse, which is similar to the results given by Settembrini et al.[14] in the study of the micro-Raman shift of a strained monolayer graphene suspended over SiN membranes micropatterned with holes of noncircular geometry. The graphene at the center of the monolayer graphene has a Raman redshift for both the G sub-bands, and the G^- sub-band for the graphene at the center of the monolayer graphene has a larger Raman redshift than the G^+ sub-band. Both trends are consistent to the observation by Settembrini et al.[14] Note that the contours of the Raman shift near the edges are present nearly in the shape of rectangle, and the graphene in this region has blueshift.

Figure 3 depicts the contours of the bending-induced Raman shift of a rectangular orthotropic graphene with two simply supported and two clamped edges under the action of a uniform pressure for $a/b = 2$, in which normalized Raman shift of $\Delta\omega_{G^{\pm}} D_1/\omega_G^0 pha^2$ is used. Similar to the bending-induced Raman shift of an orthotropic, rectangular graphene with simply supported edges, the contours of the Raman shift near the center are present approximately in the shape of ellipse, and there is a redshift around the center of the rectangular graphene and blueshift near the edge for both the G sub-bands. For the G^- sub-band, the contours of the Raman shift slightly away from the center of the graphene are present approximately in the shape of rectangle. The graphene at the center of the monolayer graphene has the largest redshift of the Raman spectra for both G sub-bands, and the G^- sub-band has a larger redshift of the Raman peak than the G^+ sub-band at the center of the monolayer graphene. The graphene near the edge has blueshift in the Raman spectrum. There exists a difference in the contour shapes between the orthotropic−

DOI: 10.1021/acs.jpcc.8b07996
J. Phys. Chem. C 2018, 122, 24467−24474

rectangular graphene with two simply supported and two clamped edges and the orthotropic−rectangular graphene of the same size with simply supported edges, which suggests that the Raman shift is dependent on the boundary conditions on the graphene.

Figure 4 shows the contours of the deformation-induced Raman shift of an orthotropic, elliptic graphene with clamped edge under the action of uniform pressure for $a/b = 2$, in which normalized Raman shift of $\Delta\omega_{G^{\pm}} D_1/\omega_G^0 pha^2$ is used. In comparison to the rectangular graphene, the contours for both G sub-bands are present in the shape of an ellipse with the cutoff for the contours near the edge of the elliptic graphene. The similarity between the contours and the shape of the elliptic graphene suggests the dependence of the Raman shift on the morphology of graphene. One may not able to use the spatial distribution of the Raman shift to suggest the anisotropic behavior of graphene, since the shape of the contours of the Raman shift is also dependent on the shape of graphene, as given by eqs 28−30. The geometric shape of the contours of the Raman shift cannot solely represent the anisotropic behavior in the mechanical deformation of the elliptic graphene. Similar to the rectangular graphene, the graphene at the center of monolayer graphene has the largest redshift of the Raman spectra for both G sub-bands, and the G^- sub-band for the graphene at the center of the monolayer graphene has a larger redshift of the Raman peak than the G^+ sub-band. There is a blueshift in the Raman spectrum for the graphene near the edge.

As discussed above, the Raman spectrum at the center of the graphene of the two geometric configurations under the action of uniform pressure has the largest Raman redshift. Figure 5 depicts the variation of the largest Raman redshift with the ratio of b/a (geometric dimensions) of the three cases under the action of uniform pressure for both the G sub-bands. For the G^+ sub-band, the largest Raman redshift increases with the increase of the ratio for the orthotropic, rectangular graphene with simply supported edges (Case I) and approaches plateau for ratios larger than or equal to 4. For the rectangular, orthotropic graphene with two simply supported edges and two clamped edges (Case II), the largest Raman redshift increases with the increase of the ratio and reaches the maximum at $b/a = 1$, then decreases with the increase of the ratio, and approaches plateau for ratios larger than or equal to 4. For the orthotropic, elliptic graphene with clamped edge (Case III), the largest Raman redshift increases with the increase of the ratio, reaches the maximum at $b/a = \sim 3.3$, then decreases with the increase of the ratio, and approaches the same plateau as that of Case II for ratio larger than 10. For the three cases, the orthotropic, rectangular graphene with simply supported edges (Case I) has the largest "largest Raman redshift" for ratio larger than 1, and the orthotropic, rectangular graphene with two simply supported edges and two clamped edges (Case II) has the largest largest Raman redshift for ratio less than 1. Such trends confirm the dependence of the Raman shift on the geometrical configurations and boundary conditions. One needs to take into account of the effect of geometrical configurations and boundary conditions in the calculation of mechanical properties of graphene via the Raman shift.

For the G^- sub-band, the largest Raman redshift increases with the increase of the ratio and approaches plateau for all three cases. The orthotropic, rectangular graphene with simply supported edges (Case I) has the largest largest Raman redshift

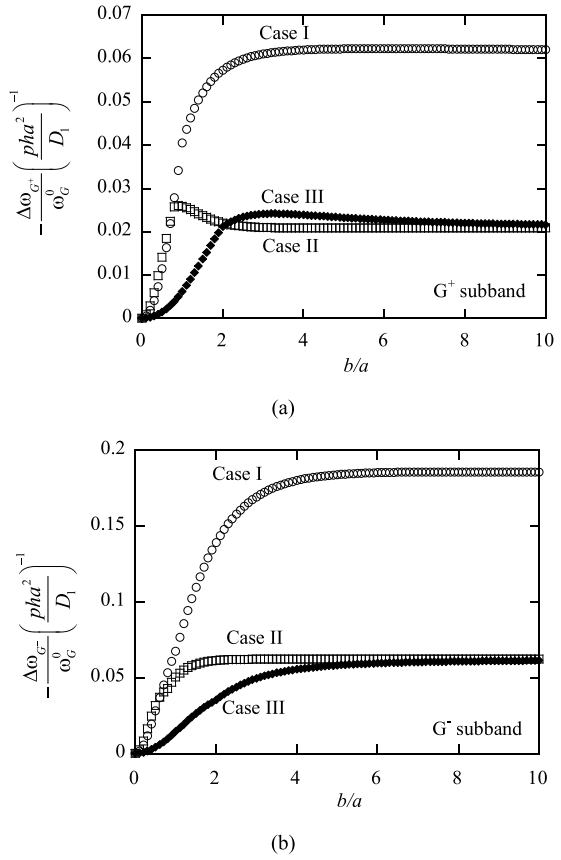

Figure 5. Variation of the bending-induced Raman shift ($\Delta\omega_{G^{\pm}} D_1/\omega_G^0 pha^2$) with ratio of b/a for all three cases; (a) G^+ sub-band and (b) G^- sub-band.

for ratio larger than ~0.6, and the orthotropic, rectangular graphene with two simply supported edges and two clamped edges (Case II) has the largest largest Raman redshift for ratio less than ~0.1. The orthotropic, elliptic graphene with clamped edge (Case III) has the smallest "the largest Raman redshift". Both the orthotropic, rectangular graphene with two simply supported edges and two clamped edges (Case II) and the orthotropic, elliptic graphene with clamped edge (Case III) approach the same plateau for large ratios of b/a. Such trends confirm the dependence of the Raman shift on the geometrical configurations and boundary conditions again.

Comparing the results in Figure 5a to those in Figure 5b, we note that the G^- sub-band has the larger "the largest Raman shift" than the G^+ sub-band under the same conditions and geometrical configuration. It would be more practical to use the Raman shift of the G^- sub-band in the applications of graphene as sensor materials.

It needs to be emphasized that the above calculation is based on graphene that is initially stress free. For initially strained graphene, eqs 10 and 11 must be used in the calculation of the Raman shift. In addition, the effect of the prestrain (prestress) needs to be taken into account in the analysis of the deformation of the graphene. For example, the deflection of an orthotropic, rectangular graphene with simply supported edges (Figure 1a), which is subjected to constant tensile stresses of q_1 and q_2 along the edges of ($x = 0, a$) and ($y = 0, b$) and uniform pressure of p, is similar to eq 19 with the coefficients of α_{mn} as[21]

DOI: 10.1021/acs.jpcc.8b07996
J. Phys. Chem. C 2018, 122, 24467−24474

$$\alpha_{mn} = \frac{(2n-1)^{-1}(2m-1)^{-1}}{D_1\left(\frac{(2m-1)b}{a}\right)^4 + 2D_3(2n-1)^2\left(\frac{(2m-1)b}{a}\right)^2 + D_2(2n-1)^4 + \chi_{mn}} \quad (31)$$

$$\chi_{mn} = \frac{b^2}{\pi^2}\left(q_1\left(\frac{(2m-1)b}{a}\right)^2 + q_2(2n-1)^2\right) \quad (32)$$

It is evident that the prestress can change the strain state of the graphene and affect the Raman shift of the peaks.

Note that the bending-induced Raman shifts are presented in dimensionless variables of $\Delta\omega_{G^\pm} D_1/\omega_G^0 pha^2$ for Figures 3−5, i.e., the only independent variables in Figures 3−5 are the spatial variables of x and y. Accordingly, the bending-induced Raman shifts of $\Delta\omega_{G^\pm}$ are proportional to the applied pressure difference p for a given spatial position. As discussed in the section of bending deformation of orthotropic graphene, the strain components are proportional to the pressure difference across the graphene. Thus, the bending-induced Raman shifts of $\Delta\omega_{G^\pm}$ are proportional to the strain in the graphene for small deformation, which exhibits the same trend as the most results reported in the literature.

SUMMARY

In summary, we have extended the relationship between the Raman shift of strained graphene and the mechanical strains under the action of uniaxial tension to three-dimensional strain state. Using this relationship, we have analyzed the bending-induced Raman shift of orthotropic, monolayer graphene of two geometrical configurations under the action of uniform pressure. The following is the summary of the results.

(1) The Raman shift of graphene is dependent on the geometrical configurations and boundary conditions.

(2) The Raman shift of graphene is dependent on the initial stress state of the graphene.

(3) The geometric shape of the contours of the Raman shift likely cannot represent anisotropic behavior in the mechanical deformation of graphene.

(4) The initial stress state of graphene needs to be known to use the Raman shift to calculate the mechanical property of graphene.

(5) The central graphene of the two geometric configurations under the action of uniform pressure has the largest Raman redshift. The rectangular, orthotropic graphene with simply supported edges has the largest largest Raman redshift for ratio larger than ∼1.

(6) The G^- sub-band has the larger "largest Raman shift" than the G^+ sub-band under the same conditions and geometrical configuration.

AUTHOR INFORMATION

Corresponding Authors

*E-mail: hchoo@caltech.edu (H.C.).
*E-mail: fyang2@uky.edu (F.Y.).

ORCID

Fuqian Yang: 0000-0001-6277-3082

Notes

The authors declare no competing financial interest.

ACKNOWLEDGMENTS

K.L.Y. is grateful for the support of Soli Deo Gloria Fellowship through the SURF program at California Institute of Technology. F.Y. is grateful for the support by the NSF through the grant CMMI-1634540, monitored by Dr. Khershed Cooper.

REFERENCES

(1) Pereira, V. M.; Neto, A. C. Strain engineering of graphene's electronic structure. *Phys. Rev. Lett.* **2009**, *103*, No. 046801.

(2) Guinea, F.; Katsnelson, M.; Geim, A. Energy gaps and a zero-field quantum Hall effect in graphene by strain engineering. *Nat. Phys.* **2010**, *6*, 30−33.

(3) Zabel, J.; Nair, R. R.; Ott, A.; Georgiou, T.; Geim, A. K.; Novoselov, K. S.; Casiraghi, C. Raman spectroscopy of graphene and bilayer under biaxial strain: bubbles and balloons. *Nano Lett.* **2012**, *12*, 617−621.

(4) Justino, C. I.; Gomes, A. R.; Freitas, A. C.; Duarte, A. C.; Rocha-Santos, T. A. Graphene based sensors and biosensors. *TrAC, Trends Anal. Chem.* **2017**, *91*, 53−66.

(5) Lazarenkova, O. L.; von Allmen, P.; Oyafuso, F.; Lee, S.; Klimeck, G. Effect of anharmonicity of the strain energy on band offsets in semiconductor nanostructures. *Appl. Phys. Lett.* **2004**, *85*, 4193−4195.

(6) Barron, T. Interatomic potentials in ideal anharmonic crystals. *Discuss. Faraday Soc.* **1965**, *40*, 69−75.

(7) Huang, M.; Yan, H.; Chen, C.; Song, D.; Heinz, T. F.; Hone, J. Phonon softening and crystallographic orientation of strained graphene studied by Raman spectroscopy. *Proc. Natl. Acad. Sci. U.S.A.* **2009**, *106*, 7304−7308.

(8) del Corro, E.; Kavan, L.; Kalbac, M.; Frank, O. Strain assessment in graphene through the Raman 2D′ mode. *J. Phys. Chem. C* **2015**, *119*, 25651−25656.

(9) Jiang, T.; Huang, R.; Zhu, Y. Interfacial sliding and buckling of monolayer graphene on a stretchable substrate. *Adv. Funct. Mater.* **2014**, *24*, 396−402.

(10) Mohiuddin, T.; Lombardo, A.; Nair, R.; Bonetti, A.; Savini, G.; Jalil, R.; Bonini, N.; Basko, D.; Galiotis, C.; Marzari, N.; et al. Uniaxial strain in graphene by Raman spectroscopy: G peak splitting, Grüneisen parameters, and sample orientation. *Phys. Rev. B* **2009**, *79*, No. 205433.

(11) Lee, J.-U.; Yoon, D.; Cheong, H. Estimation of Young's modulus of graphene by Raman spectroscopy. *Nano Lett.* **2012**, *12*, 4444−4448.

(12) Androulidakis, C.; Koukaras, E. N.; Parthenios, J.; Kalosakas, G.; Papagelis, K.; Galiotis, C. Graphene flakes under controlled biaxial deformation. *Sci. Rep.* **2015**, *5*, No. 18219.

(13) Ni, Z.; Bu, H.; Zou, M.; Yi, H.; Bi, K.; Chen, Y. Anisotropic mechanical properties of graphene sheets from molecular dynamics. *Phys. B* **2010**, *405*, 1301−1306.

(14) Settembrini, F. F.; Colangelo, F.; Pitanti, A.; Miseikis, V.; Coletti, C.; Menichetti, G.; Colle, R.; Grosso, G.; Tredicucci, A.; Roddaro, S. Anisotropic straining of graphene using micropatterned SiN membranes. *APL Mater.* **2016**, *4*, No. 116107.

(15) Dastjerdi, S.; Jabbarzadeh, M. Nonlinear bending analysis of bilayer orthotropic graphene sheets resting on Winkler−Pasternak elastic foundation based on non-local continuum mechanics. *Composites, Part B* **2016**, *87*, 161−175.

(16) Mohammadi, M.; Farajpour, A.; Moradi, A.; Ghayour, M. Shear buckling of orthotropic rectangular graphene sheet embedded in an elastic medium in thermal environment. *Composites, Part B* **2014**, *56*, 629−637.

(17) Galiotis, C.; Frank, O.; Koukaras, E. N.; Sfyris, D. Graphene mechanics: current status and perspectives. *Annu. Rev. Chem. Biomol. Eng.* **2015**, *6*, 121−140.

(18) Young, R. J.; Kinloch, I. A.; Gong, L.; Novoselov, K. S. The mechanics of graphene nanocomposites: a review. *Compos. Sci. Technol.* **2012**, *72*, 1459−1476.

DOI: 10.1021/acs.jpcc.8b07996
J. Phys. Chem. C 2018, 122, 24467−24474

(19) Frank, O.; Mohr, M.; Maultzsch, J.; Thomsen, C.; Riaz, I.; Jalil, R.; Novoselov, K. S.; Tsoukleri, G.; Parthenios, J.; Papagelis, K.; et al. Raman 2D-band splitting in graphene: theory and experiment. *ACS Nano* **2011**, *5*, 2231−2239.
(20) Narula, R.; Reich, S. Probing LO phonons of graphene under tension via the 2 D′ Raman mode. *Phys. Rev. B* **2013**, *87*, No. 115424.
(21) Panc, V. *Theories of Elastic Plates*; Springer: Netherlands, 1975; Vol. 2.
(22) Liu, X.; Metcalf, T. H.; Robinson, J. T.; Houston, B. H.; Scarpa, F. Shear modulus of monolayer graphene prepared by chemical vapor deposition. *Nano Lett.* **2012**, *12*, 1013−1017.

DOI: 10.1021/acs.jpcc.8b07996
J. Phys. Chem. C 2018, 122, 24467−24474